Velocity, energy, and helicity of vortex knots and unknots

F. Maggioni,[1] S. Alamri,[2] C. F. Barenghi,[3] and R. L. Ricca[4]
[1]*Department of Mathematics, Statistics, Computer Science and Applications, University of Bergamo, Via dei Caniana 2, 24127 Bergamo, Italy*
[2]*Department of Applied Mathematics, College of Applied Science, Taibah University, P.O. Box 344, Al-Madinah Al-Munawarah, Saudi Arabia*
[3]*School of Mathematics and Statistics, Newcastle University, Newcastle upon Tyne NE1 7RU, United Kingdom*
[4]*Department of Mathematics and Applications, University of Milano-Bicocca, Via Cozzi 53, 20125 Milano, Italy*
(Received 21 February 2010; revised manuscript received 9 July 2010; published 17 August 2010)

In this paper we determine the velocity, the energy, and estimate writhe and twist helicity contributions of vortex filaments in the shape of torus knots and unknots (as toroidal and poloidal coils) in a perfect fluid. Calculations are performed by numerical integration of the Biot-Savart law. Vortex complexity is parametrized by the winding number w given by the ratio of the number of meridian wraps to that of longitudinal wraps. We find that for $w<1$ vortex knots and toroidal coils move faster and carry more energy than a reference vortex ring of same size and circulation, whereas for $w>1$ knots and poloidal coils have approximately same speed and energy of the reference vortex ring. Helicity is dominated by writhe contributions. Finally, we confirm the stabilizing effect of the Biot-Savart law for all knots and unknots tested, found to be structurally stable over a distance of several diameters. Our results also apply to quantized vortices in superfluid ^{4}He.

DOI: 10.1103/PhysRevE.82.026309 PACS number(s): 47.32.cd, 47.37.+q, 67.25.dk

I. INTRODUCTION

The study of vortex filament motion in an ideal fluid, and in particular of vortex rings in presence or absence of periodic displacements of the vortex axis from the circular shape (Kelvin waves), dates back to the late 1800s [1,2]. Despite this long history, this study is still an active area of research [3–5]. For example, the fact that upon large amplitude Kelvin waves vortex rings can slow down and even reverse their translational motion has been recognized only recently [6–8]. Alongside the traditional interest for problems in classical fluid mechanics, additional interest is motivated by current work on superfluid helium [9–12] and atomic Bose-Einstein condensates [13–15].

Here we shall be concerned with slightly more complex vortex structures; namely vortex filaments in the shape of torus knots and unknots in an ideal fluid. Since these vortices are closely related to circular vortex filaments with small-amplitude distortions on a mathematical torus, they propagate in the fluid like vortex rings, by self-induction along the central axis of the torus, and they also rotate in the meridian plane (the poloidal plane of the torus) as their vortex core spins around the local center of mass, inducing an additional twist motion of the vortex around itself, that cannot be neglected.

Among all possible knot types, torus knots constitute a special family of knots amenable to particularly simple mathematical description. These knots can be described by closed curves wound on a mathematical torus, p times in the longitudinal direction and q times in the meridian direction of the torus. If $p>1$ and $q>1$ are coprime integers, then we have standard torus knots (see Fig. 1), whereas if the curve winds the torus only once in either directions, then the curve is unknotted (see Fig. 2). If $p=q=1$ the curve is the standard circle. Even though the topology of unknots is trivial, the geometry may become rather complex, taking the shape of toroidal or poloidal coil, according to which direction the curve is multiply wound.

Vortex torus knots and unknots provide a good example of relatively complex structures, where relationships between dynamical properties such as velocity and energy, and geometric and topological features, can be determined. The aim of this paper is thus to continue and extend previous work [16,17] toward the study of more complex vortex structures present in turbulent flows. Here we shall investigate the propagation velocity and the kinetic energy of vortex torus knots and unknots in some generality, by comparing results to a standard vortex ring of same size. Since superfluid ^{4}He has zero viscosity, thus providing a realistic example of an Euler fluid, we shall choose circulation and vortex core radius as physically realistic quantities for quantized vortices in superfluid helium, and we shall carry out this research by direct numerical integration of the Biot-Savart law. Unlike previous vortex dynamics calculations of quantized vorticity

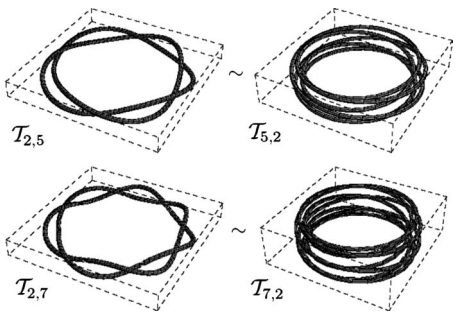

FIG. 1. Examples of torus knots with winding number $w>1$ (on the left) and $w<1$ (on the right). For given p and q, any torus knot $\mathcal{T}_{p,q}$ can be continuously deformed to its topologically equivalent alternative form $\mathcal{T}_{q,p}$; the two knots have different geometry, but same topology, thus $\mathcal{T}_{p,q}\sim\mathcal{T}_{q,p}$. Three-dimensional visualization of each knot is enhanced by centering a mathematical tube on the knot axis.

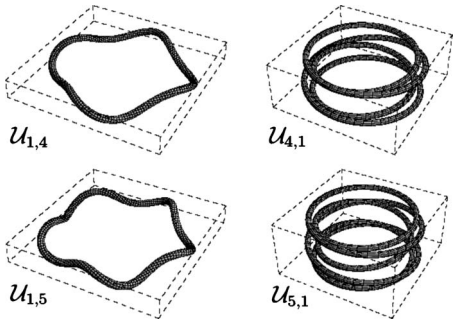

FIG. 2. Examples of torus unknots with winding number $w>1$ (poloidal coils; on the left) and $w<1$ (toroidal coils; on the right). These unknots can be transformed to the standard circle by continuous deformations, thus they are all equivalent to the unknot. Three-dimensional visualization is enhanced by centering a mathematical tube on the curve axis.

[18–21], however, we shall assume that no friction force [22] acts on the superfluid vortices; thus our results will apply to superfluid helium at temperatures below 1 K, where the dissipative effects of the normal fluid are truly negligible.

II. MATHEMATICAL BACKGROUND

A. Vortex motion under the Biot-Savart and the LIA law

We consider vortex motion in an ideal, incompressible fluid, in an unbounded domain. The velocity field $\mathbf{u}=\mathbf{u}(\mathbf{x},t)$, smooth function of the vector position $\mathbf{x}$ and time t, satisfies

$$\nabla\cdot\mathbf{u}=0 \quad \text{in } \mathbb{R}^3, \quad \mathbf{u}\to\mathbf{0} \quad \text{as } \mathbf{x}\to\infty, \tag{1}$$

with vorticity $\boldsymbol{\omega}$ defined by

$$\boldsymbol{\omega}=\nabla\times\mathbf{u}, \quad \nabla\cdot\boldsymbol{\omega}=0 \quad \text{in } \mathbb{R}^3. \tag{2}$$

In absence of viscosity, fluid evolution is governed by the Euler equations and vortex motion obeys Helmholtz's conservation laws [23]. Transport of vorticity is given by

$$\frac{\partial\boldsymbol{\omega}}{\partial t}=\nabla\times(\mathbf{u}\times\boldsymbol{\omega}), \tag{3}$$

admitting formal solutions in terms of the Cauchy equations

$$\omega_i(\mathbf{x},t)=\omega_j(\mathbf{a},0)\frac{\partial x_i}{\partial \mathrm{a}_j}. \tag{4}$$

From this expression we can see how both convection of vorticity from the initial position $\mathbf{a}$ to the final position $\mathbf{x}$, and the simultaneous rotation and distortion of the vortex elements by the deformation tensor $\partial x_i/\partial \mathrm{a}_j$ are combined together. Since this tensor is associated with a continuous deformation of the vortex elements (by the diffeomorphism of the flow map), vorticity is thus mapped continuously from its initial configuration $\boldsymbol{\omega}(\mathbf{a},0)$ to the final state given by $\boldsymbol{\omega}(\mathbf{x},t)$; hence the Cauchy equations establish a topological equivalence between initial and final configuration by preserving vorticity topology. In absence of dissipation, physical properties such as kinetic energy, helicity, and momenta are also conserved, together with topological quantities such as knot type, minimum crossing number and self-linking number [24].

The kinetic energy per unit density E is given by

$$E=\frac{1}{2}\int_V \|\mathbf{u}\|^2 d^3\mathbf{x}=\text{constant}, \tag{5}$$

and the kinetic helicity H by

$$H=\int_V \mathbf{u}\cdot\boldsymbol{\omega}\, d^3\mathbf{x}=\text{constant}, \tag{6}$$

where V is the domain volume of vorticity. Here we assume to have only one vortex filament $\mathcal{F}$ in isolation, where $\mathcal{F}$ is centered on the curve $\mathcal{C}$ of equation $\mathbf{X}=\mathbf{X}(s)$ (s being the arc-length of $\mathcal{C}$). The filament axis $\mathcal{C}$ is given by a smooth space curve $\mathcal{C}$ without self-intersections. The filament volume is given by $V(\mathcal{F})=\pi a^2 L$, where $L=L(\mathcal{C})$ is the total length of $\mathcal{C}$ and a is the radius of the vortex core, assumed to be uniformly circular all along $\mathcal{C}$ and much smaller than any length scale of interest in the flow (thin-filament approximation); this assumption is relevant (and particularly realistic) in the context of superfluid helium vortex dynamics, where typically $a\approx 10^{-8}$ cm.

Vortex motion is governed by the Biot-Savart law (BS for short) given by

$$\mathbf{u}(\mathbf{x})=\frac{\Gamma}{4\pi}\oint_{\mathcal{C}}\frac{\hat{\mathbf{t}}(s)\times[\mathbf{x}-\mathbf{X}(s)]}{\|\mathbf{x}-\mathbf{X}(s)\|^3}ds, \tag{7}$$

where Γ is the vortex circulation due to $\boldsymbol{\omega}=\omega_0\hat{\mathbf{t}}$, where ω_0 is a constant and $\hat{\mathbf{t}}(s)=d\mathbf{X}/ds$ the unit tangent to $\mathcal{C}$. Since the Biot-Savart integral is a global functional of the vorticity, analytical solutions in closed form other than the classical solutions associated with rectilinear, circular and helical geometry are very difficult to obtain. Considerable analytical progress, however, has been done by using the Localized Induction Approximation (LIA for short) law. This equation, first derived by Da Rios [25] and independently rediscovered by Arms and Hama [26] (see the review by Ricca [27]), is obtained by a Taylor's expansion of the Biot-Savart integrand from a point on $\mathcal{C}$ (see, for example, the derivation by Batchelor [28]). By ignoring the rotational component of the self-induced velocity (that in any case does not contribute to the displacement of the vortex filament in the fluid) and nonlocal terms, the LIA equation takes the simplified form

$$\mathbf{u}_{\mathrm{LIA}}=\frac{\Gamma c}{4\pi}\ln(\delta)\hat{\mathbf{b}}\propto c\hat{\mathbf{b}}, \tag{8}$$

where $c=c(s)$ is the local curvature of $\mathcal{C}$, δ is a measure of the aspect ratio of the vortex, given by the radius of curvature divided by the vortex core radius and $\hat{\mathbf{b}}=\hat{\mathbf{b}}(s)$ the unit binormal vector to $\mathcal{C}$.

B. Torus knots

We consider a particular family of vortex configurations in the shape of torus knots in $\mathbb{R}^3$. These are given when the curve $\mathcal{C}$ takes the shape of a torus knot $\mathcal{T}_{p,q}$ ($\{p,q\}$ coprime

integers, with $p>1$ and $q>1$), given by a closed curve wound on a mathematical torus p times in the longitudinal (toroidal) direction and q times in the meridian (poloidal) direction (see Fig. 1). When one of the integers is equal to 1 and the other to m, the curve is no longer knotted, but it becomes an unknot, homeomorphic to the standard circle $\mathcal{U}_0$, with a complex geometry. Depending on which index takes the value m, the curve takes the shape of toroidal coil ($p=m$) $\mathcal{U}_{m,1}$, or poloidal coil ($q=m$) $\mathcal{U}_{1,m}$ (see Fig. 2). When $\{p,q\}$ are both rational, then $\mathcal{T}_{p,q}$ is no longer a closed knot, and the curve covers the toroidal surface completely. Here we shall consider only curves given by $\{p,q\}$ integers. For given p and q, the knot $\mathcal{T}_{p,q}$ can be transformed by continuous deformations to the alternative form $\mathcal{T}_{q,p}$: hence the knots $\mathcal{T}_{p,q}$ and $\mathcal{T}_{q,p}$ represent the same knot type: the two knots have different geometry, but they are topologically equivalent, and we write $\mathcal{T}_{p,q}\sim\mathcal{T}_{q,p}$.

Unknots such as toroidal coils may be used to study the motion of thick vortex rings with internal swirl flow given by one full turn of twist of vorticity in the vortex core; poloidal coils, on the other hand, may provide a model of toroidal jets.

Now, let us identify each curve with a vortex filament; hence, we shall refer to $\mathcal{T}_{p,q}$ as a vortex torus knot and consider its dynamics and energy by using the BS law [Eq. (7)] and the LIA law [Eq. (8)] to explore the effects of the geometry and topology on the dynamical and the energetic properties of the vortex.

The existence of torus knot solutions to LIA were found by Kida [29] in terms of elliptic integrals. By rewriting LIA in cylindrical polar coordinates (r,α,z), and by using standard linear perturbation techniques, small-amplitude torus knot solutions (asymptotically equivalent to Kida's solutions) were derived by Ricca [30]. These latter give solution curves explicitly in terms of the arc-length s,

$$\begin{cases} r = r_0 + \epsilon \sin(w\phi), \\ \alpha = \dfrac{s}{r_0} + \dfrac{\epsilon}{w r_0}\cos(w\phi), \\ z = \dfrac{t}{r_0} + \epsilon\left(1+\dfrac{1}{w^2}\right)^{1/2}\cos(w\phi), \end{cases} \tag{9}$$

where r_0 is the radius of the torus circular axis, $\epsilon\ll 1$ is the inverse of the aspect ratio of the vortex and $w=q/p$ the *winding number* of the curve. Since the LIA is related to the one-dimensional nonlinear Schrödinger equation (NLSE) [27], torus knot solutions [Eqs. (9)] correspond to helical traveling waves propagating along the filament axis, with wave speed κ and phase $\phi=(s-\kappa t)/r_0$. Thus, vortex motion under LIA is given by a rigid body translation and rotation, with translation velocity $u=\dot{z}$ along the torus central axis, and a uniform helical motion along the circular axis of the torus given by radial and angular velocity components $\dot{r}$ and $\dot{\alpha}$. In physical terms, these waves provide an efficient mechanism for the transport of kinetic energy and momenta throughout the fluid.

By using Eqs. (9), Ricca [31] proved the following linear stability result:

Theorem 1. Let $\mathcal{T}_{p,q}$ be a small-amplitude vortex torus knot under LIA. Then $\mathcal{T}_{p,q}$ is steady and stable under linear perturbations if and only if $q>p$ $(w>1)$.

This result provides a criterium for LIA stability of vortex knots, and it can be easily extended to inspect stability of torus unknots (i.e., toroidal and poloidal coils). This stability result has been confirmed for several knot types tested by numerical experiments [17]. LIA unstable torus knot was found to be stabilized under the BS law, presumably because of the global induction effects of the vortex: indeed, nearby parts of different strands of the vortex filament rotate around each other in the meridian plane, orbiting uniformly around the torus circular axis, thus providing an effect that induces a more uniform velocity field. It is this global effect, absent under the LIA law, and due to the local and nonlocal contributions to the BS law, that appears to enhance the stability of the translational motion of the vortex knot.

C. Measures of structural complexity

The winding number $w=q/p$ and the *self-linking number* $Lk=pq$ are two topological invariants of $\mathcal{T}_{p,q}$, thus they are conserved under vortex evolution. Two useful measures of geometric complexity of the vortex filament in space are given by the *writhing number Wr* and the *total twist number Tw* [32]. The writhing number is defined by

$$Wr = \frac{1}{4\pi}\oint_{\mathcal{C}}\oint_{\mathcal{C}} \frac{\hat{\mathbf{t}}(s)\times\hat{\mathbf{t}}(s^*)\cdot[\mathbf{X}(s)-\mathbf{X}(s^*)]}{\|\mathbf{X}(s)-\mathbf{X}(s^*)\|^3} ds\, ds^*, \tag{10}$$

where $\mathbf{X}(s)$ and $\mathbf{X}(s^*)$ denote two points on the curve $\mathcal{C}$ for any pair $\{s,s^*\}\in[0,L]$. The writhing number provides information on the amount of total coiling and distortion of the filament *axis* in space. The total twist number Tw may be written as [33]

$$Tw = \frac{1}{2\pi}\oint_{\mathcal{C}}\left(\frac{d\hat{\mathbf{n}}}{ds}\times\hat{\mathbf{n}}\right)\cdot\hat{\mathbf{t}}\,ds = \frac{1}{2\pi}\oint_{\mathcal{C}}\left(\tau+\frac{d\Theta}{ds}\right)ds, \tag{11}$$

where the rotation rate of $\hat{\mathbf{n}}=\hat{\mathbf{n}}(s)$ (the unit normal to $\mathcal{C}$) around the filament axis, provides a combined measure of torsion $\tau=\tau(s)$ and internal twist $\Theta=\Theta(s)$ of the vorticity. Tw is indeed a good measure of the total torsion and internal twist of the vortex filament in space. Since the self-linking number Lk can be expressed as the sum of Wr and Tw (Călugăreanu–White formula), the kinetic helicity H of vortex torus knots $\mathcal{T}_{p,q}$ can be written as [33]

$$H = Lk\Gamma^2 = pq\Gamma^2 = (Wr+Tw)\Gamma^2, \tag{12}$$

encompassing in a single expression, by Eq. (6), dynamical and geometric aspects of vortex motion. The right-hand-side of the above equation provides a straightforward estimate of kinetic helicity by avoiding the direct calculation of the integral [Eq. (6)].

For the unknots, however, we should set $Lk=0$, in agreement with the standard vortex ring values of $Wr=0$ and $Tw=0$. Hence, for the unknots we have $Wr=-Tw$.

Since under LIA the internal twist $\Theta=0$ everywhere along $\mathcal{C}$, then in this case total twist reduces to total torsion and

each term of Eq. (12) becomes proportional to global geometric quantities, that is [31]

$$H \propto \oint_{\mathcal{C}} c^2 \tau \, ds, \quad Wr \propto \oint_{\mathcal{C}} c^2 ds, \quad Tw \propto \oint_{\mathcal{C}} \tau \, ds, \quad (13)$$

that are now conserved, corresponding with the first few soliton invariants of the associated NLSE.

III. NUMERICAL METHOD

All the dynamical quantities of vortex knots and unknots are evaluated by direct numerical integration of the BS law [Eq. (7)] and direct numerical calculation of the other properties. The numerical code is described in detail elsewhere [34], and it has been used also to study interaction and reconnection of vortex bundles [35]. The vortex axis is discretized into N segments and the Biot-Savart integral is desingularized by application of a standard cutoff technique [18,20,34]. The time evolution is realized by using a fourth order Runge-Kutta algorithm. Convergence has been tested in space and time as usual, by modifying the number of discretization points and the size of the time step.

The initial condition is given by Eq. (9), where we have set $r_0=1$ cm, $\epsilon=0.1$, $\Gamma=10^{-3}$ cm^2/s, (the value expected for superfluid ^{4}He), $\delta=2\times10^8/e^{1/2}\gg1$ (typical of a superfluid helium vortex core radius $a=10^{-8}$ cm). To investigate the behavior of the unknots the term $(1-1/w^2)$ in Eqs. (9) is replaced by $|1-1/w^2|$. It is useful to compare these results with the dynamics of a vortex ring $\mathcal{U}_0$ of same size and vorticity. Thus we take a reference vortex ring of radius $r_0=1$ cm. The typical time step value in our calculations is 10^{-2} s. Convergence in time has been tested by ranging the time step from 10^{-3} s to 5×10^{-2} s. Two examples of convergence in space are shown in Fig. 3 for the torus knot $\mathcal{T}_{2,5}$ and the unknot $\mathcal{U}_{4,1}$. The calculations are performed using constant mesh density N/L chosen following convergence tests similar to those shown in Fig. 3. We have set $N/L=50$ for poloidal unknots $\mathcal{U}_{1,m}$ $(m=2,3,\ldots,7)$, $N/L=20$ for toroidal unknots $\mathcal{U}_{m,1}$ $(m=2,3,\ldots,7)$, $N/L=30$ for knots $\mathcal{T}_{2,q}$ $(q=3,5,7,9)$ and $N/L=7$ for knots $\mathcal{T}_{p,2}$ $(p=3,5,7,9)$. Typical errors in computing the velocity and the energy are of the order of 10^{-5} cm/s and 10^{-7} cm^5/s^2, respectively. For the reference vortex ring we have set $w=1$ and $N=313$; then $L=6.26$ cm and $N/L=50$, with translational velocity $u_0=1.38\times10^{-3}$ cm/s, kinetic energy $E_0=8.77\times10^{-6}$ cm^5/s^2 and zero helicity.

IV. RESULTS: GEOMETRIC PROPERTIES, VELOCITY, ENERGY AND HELICITY

Numerical values of calculated quantities are reported on Tables I and II. Since geometric properties influence the velocity, the energy and the helicity of vortex structures, it is important to consider these first.

A. Total length, writhing and total twist number

Diagrams of total length and writhing of knots and unknots are shown in Fig. 4. The diagrams of total length reflect the elementary fact that the longitudinal wraps contribute to total length more than the meridian wraps. The marked difference in the slope of the two plots in each diagram is due to the dominant contribution to L by the longitudinal wraps compared to that of the meridian wraps. Similar behavior is reflected in the kinetic energy of the system.

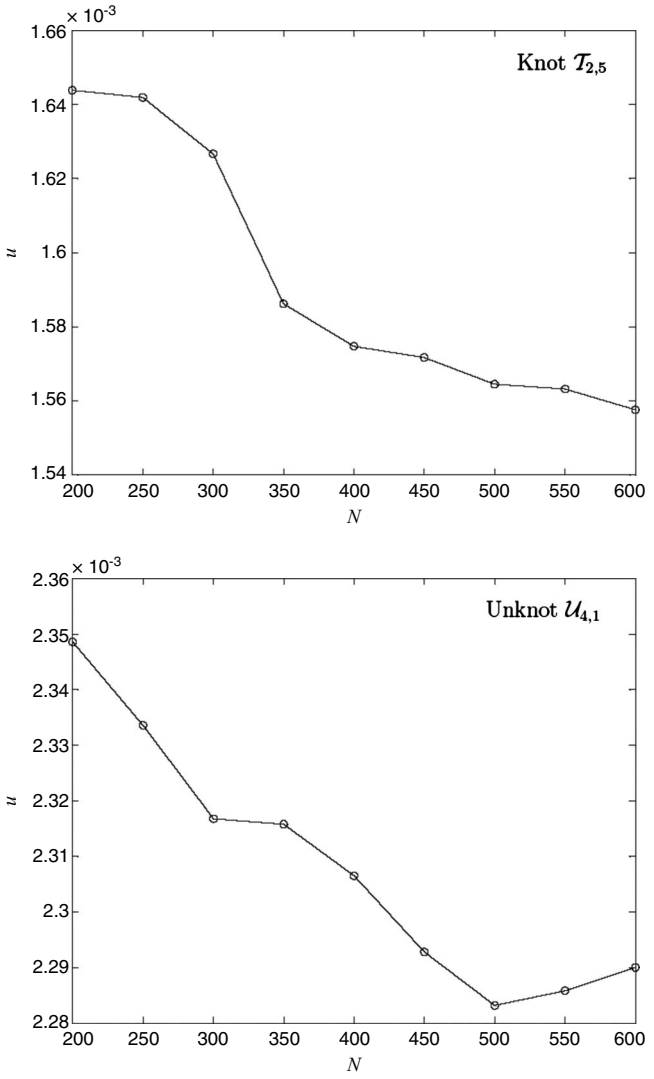

FIG. 3. Two examples of convergence test given by plots of the translational velocity u against the number N of discretization points on the vortex axis. Similar results have been found for all knots/unknots tested. Connecting lines are only for visualization purposes.

Similarly for the amount of coiling and distortion of the filament axis measured by the writhing number Wr. As we can see from the diagrams of Fig. 4, meridian wraps contribute modestly to the total writhing of the filament, the dominant contribution coming from the longitudinal wraps. In this case, however, the effects of distortion due to the presence of meridian wraps are appreciable, especially for the $\mathcal{T}_{2,q}$ knots. Moreover, since the self-linking Lk of the vortex filament is a topologically conserved quantity, for torus knots we have $Tw=Lk-Wr=pq-Wr$ and for unknots $Tw=-Wr$, allowing direct computation of the total twist. Values of Tw are shown on Tables I and II. As expected, we see that in absolute value

TABLE I. Vortex knots: calculated numerical values; entries in the last column (Y/N) report whether or not a reconnection event has taken place on or before time t.

p	q	w	N	L (cm)	N/L	Wr	Tw	u (cm/s)	E (cm^5/s^2)	E/L (cm^4/s^2)	z (cm)	t (s)	Rec.
2	3	1.5	378	12.6	30	3.01	2.99	1.66×10^{-3}	0.19×10^{-4}	0.15×10^{-5}	8.9	5300	N
2	5	2.5	385	12.9	30	5.11	4.89	1.57×10^{-3}	0.20×10^{-4}	0.16×10^{-5}	14	8800	Y
2	7	3.5	397	13.2	30	7.31	6.69	1.55×10^{-3}	0.20×10^{-4}	0.15×10^{-5}	13	8000	N
2	9	4.5	411	13.7	30	9.74	8.26	1.47×10^{-3}	0.21×10^{-4}	0.15×10^{-5}	8	5400	Y
3	2	0.7	131	18.8	7	3.99	2.01	2.04×10^{-3}	0.33×10^{-4}	0.18×10^{-5}	33	16000	Y
5	2	0.4	219	31.3	7	7.98	2.02	2.65×10^{-3}	0.67×10^{-4}	0.21×10^{-5}	15	5800	Y
7	2	0.3	307	43.9	7	12.0	2.0	3.24×10^{-3}	1.10×10^{-4}	0.25×10^{-5}	1	320	Y
9	2	0.2	395	56.4	7	16.0	2.0	3.81×10^{-3}	1.60×10^{-4}	0.28×10^{-5}	0.4	110	Y

the twist increases with the number of meridian wraps. From these values and by Eq. (12) we have an immediate information on the relative contributions to the kinetic helicity (see the discussion in the subsection below).

B. Translation velocity

The translational velocity $u=\dot{z}$ along the central axis of knots and unknots is calculated by using the Biot-Savart law. Absolute values are reported on Tables I and II. The diagrams of Fig. 5 show the normalized velocity u/u_0 of knots and unknots plotted against the winding number, where u_0 denotes the translational velocity of the reference vortex ring. The normalized velocity is greatly influenced by the relative number of longitudinal wraps, which contribute greatly to the total curvature of the vortex. In general the velocity decreases with increasing winding number. Fastest vortex systems are torus knots with highest number of longitudinal wraps. In the case of unknots we can see that meridian wraps actually slow down poloidal coils $\mathcal{U}_{1,m}$, making them traveling slower than the corresponding vortex ring. This trend reveals that at very high winding number, torus knots, and poloidal coils tend to reverse their velocity, thus traveling backward in space. This curious phenomenon has been observed independently [6,7], and it can be justified on theoretical grounds by information based on structural complexity analysis [8,36].

An estimate of the relationship between normalized velocity u/u_0 and winding number w of torus knots is obtained by a linear regression, given by

$$u/u_0 = \begin{cases} 4.41 - 9.13w + 7.09w^2, & (w < 1), \\ 1.25 - 0.04w, & (w > 1), \end{cases} \tag{14}$$

with standard deviation of 0.031.

In the limit $w \to 0$, the knot covers the toroidal surface completely with an infinite number of longitudinal wraps, and vorticity becomes a sheet of toroidal vorticity, with the induced velocity purely poloidal in the interior and exterior region of the torus, that jumps across the sheet in opposite directions. The regression [Eq. (14)] suggests a theoretical limit value $u/u_0=4.41$ that seems to be independent of the aspect ratio of the torus. In the other limit, $w \to \infty$, the knot

TABLE II. Vortex unknots: calculated numerical values; entries in the last column (Y/N) report whether or not a reconnection event has taken place on or before time t.

p	q	w	N	L (cm)	N/L	Wr	Tw	u (cm/s)	E (cm^5/s^2)	E/L (cm^4/s^2)	z (cm)	t (s)	Rec.
1	2	2	318	6.4	50	0.02	−0.02	1.35×10^{-3}	0.09×10^{-4}	0.14×10^{-5}	11	8100	N
1	3	3	325	6.5	50	0.11	−0.11	1.30×10^{-3}	0.09×10^{-4}	0.14×10^{-5}	31	23000	N
1	4	4	336	6.7	50	0.26	−0.26	1.23×10^{-3}	0.09×10^{-4}	0.14×10^{-5}	8.3	6700	N
1	5	5	349	7.0	50	0.50	−0.50	1.15×10^{-3}	0.10×10^{-4}	0.14×10^{-5}	24	20000	N
1	6	6	365	7.3	50	0.83	−0.83	1.06×10^{-3}	0.10×10^{-4}	0.14×10^{-5}	75	7200	N
1	7	7	390	7.6	50	1.24	−1.24	0.96×10^{-3}	0.10×10^{-4}	0.13×10^{-5}	0.2	160	N
2	1	0.5	250	12.5	20	0.99	−0.99	1.69×10^{-3}	0.19×10^{-4}	0.15×10^{-5}	10	5900	Y
3	1	0.3	376	18.8	20	1.99	−1.99	2.01×10^{-3}	0.32×10^{-4}	0.17×10^{-5}	20	9700	Y
4	1	0.2	500	25.1	20	2.98	−2.98	2.28×10^{-3}	0.48×10^{-4}	0.19×10^{-5}	7.1	3100	Y
5	1	0.2	627	31.3	20	3.98	−3.98	2.58×10^{-3}	0.65×10^{-4}	0.21×10^{-5}	15	5800	Y
6	1	0.2	752	37.6	20	4.97	−4.97	2.84×10^{-3}	0.84×10^{-4}	0.22×10^{-5}	0.2	70	N
7	1	0.1	878	43.9	20	5.97	−5.97	3.09×10^{-3}	1.00×10^{-4}	0.23×10^{-5}	0.2	50	N

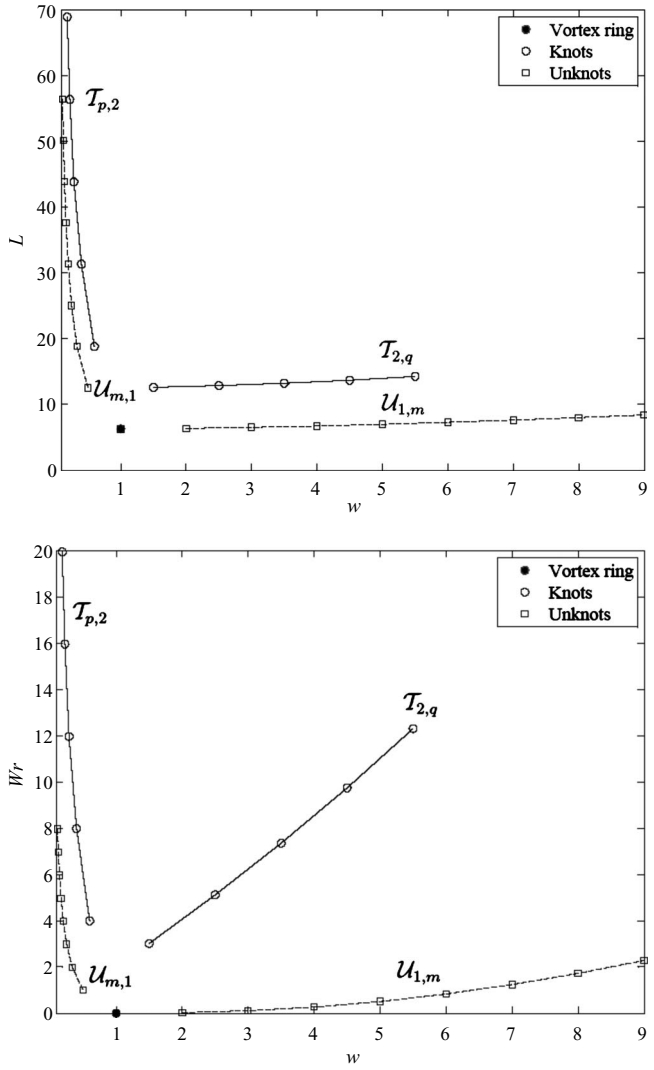

FIG. 4. Total length L and writhing number Wr plotted against the winding number w of torus knots and unknots tested ($p=3,5,7,9$; $q=3,5,7,9$; $m=2,3,\ldots,7$). The isolated black circle denotes the reference vortex ring value. Connecting lines are for visualization purposes only.

covers the torus with an infinite number of meridian wraps, and in this case vorticity induces a toroidal jet in the interior region.

C. Kinetic energy

The diagrams of the normalized kinetic energy per unit density E/E_0 plotted against the winding number w are shown in Fig. 6. Calculations are done by using the Biot-Savart law (E_{BS}/E_0) and the LIA law (E_{LIA}/E_0). The trends are dictated by the behavior of total length $L=L(w)$ (cf. the diagrams of Fig. 4). Here the calculation of the volume integral [Eq. (5)] is replaced by the (computationally convenient) line integral [37]

$$E_{\mathrm{BS}} = \frac{\Gamma}{2}\oint_C \mathbf{u}\cdot\mathbf{X}\times\mathbf{t}\, ds. \tag{15}$$

An estimate of the relationship between the normalized energy E_{BS}/E_0 of torus knots and their winding number w is

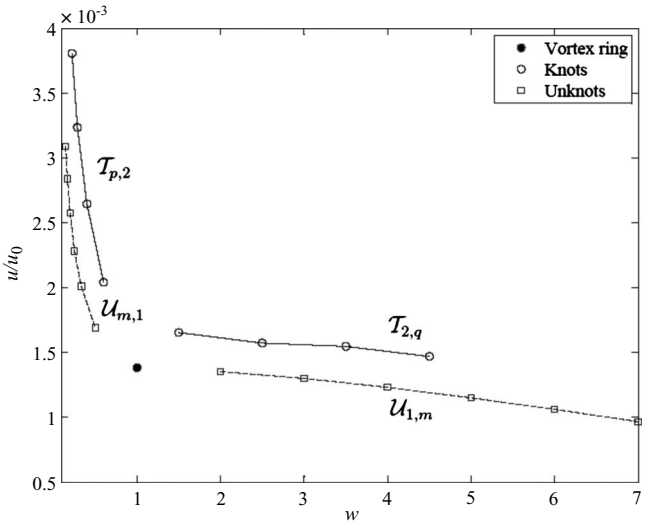

FIG. 5. Normalized translational velocity u/u_0 plotted against the winding number w of the torus knots and unknots tested ($p=3,5,7,9$; $q=3,5,7,9$; $m=2,3,\ldots,7$). The isolated black circle denotes the reference vortex ring value. Connecting lines are for visualization purposes only.

given by a nonlinear regression based on least-squares,

$$E_{\mathrm{BS}}/E_0 = 2.35 + 67.03e^{-6.44w}, \quad (w<1), \tag{16}$$

with root mean square deviation of 0.218.

A marked difference in these trends is obtained by calculating the normalized energy by using the LIA law; in this case, by using Eq. (8), we have

$$E_{\mathrm{LIA}} = \frac{1}{2}\int_V \|\mathbf{u}_{\mathrm{LIA}}\|^2 d^3\mathbf{x} = \left(\frac{\Gamma \ln \delta}{4\pi}\right)^2 \oint_C c^2 ds, \tag{17}$$

that is one of the conserved quantities associated with the LIA law [30]. Direct comparison between the diagrams of the two energies reveals such different behaviors: for $w<1$ the LIA law underestimates the actual energy of the vortex (knotted or unknotted), whereas for $w>1$ the LIA provides much higher energy values. There are two distinct reasons for this: (i) torsion and higher-order local effects ignored by LIA; (ii) nonlocal effects due to nearby vortex strands also ignored by LIA. The LIA energy of $\mathcal{T}_{9,2}$ and $\mathcal{U}_{7,1}$, for example, is about 40% less than the corresponding BS energy, whereas $\mathcal{T}_{2,9}$ and $\mathcal{U}_{1,7}$ under LIA have 3 and 14 times more energy than their corresponding BS counterparts. Since higher-order local effects (including torsion and geometric gradients) are effectively of second-order importance in the dynamics, these differences are essentially due to the contributions from the induction effects of nearby strands, captured by the BS law, but completely ignored under LIA.

Another quantity of interest is the kinetic energy per unit length E/L. From the Tables I and II we see that for $w<1$ E/L can almost double. This result has interesting implications for the interpretation of experiments on superfluid turbulence, particularly at low temperatures, a regime that is dominated by Kelvin waves [38]. What is measured in the experiments is the total vortex length per unit volume Λ, and

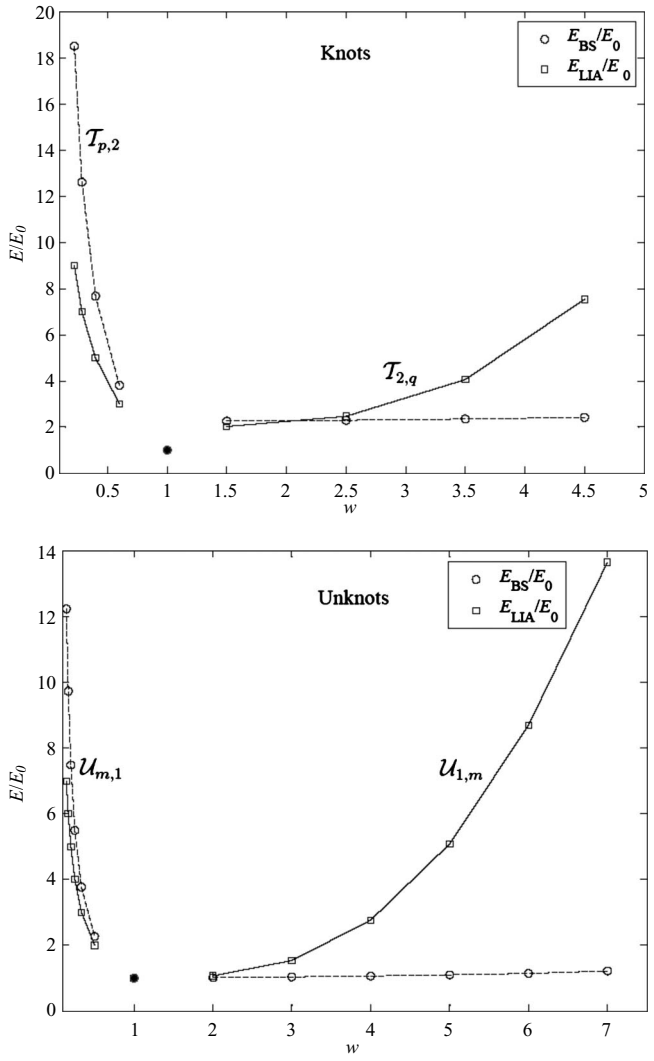

FIG. 6. Normalized kinetic energy E/E_0 calculated by using the Biot-Savart law (E_{BS}/E_0) and the LIA law (E_{LIA}/E_0), plotted against the winding number w of the knots and unknots tested ($p=3,5,7,9$; $q=3,5,7,9$; $m=2,3,\ldots,7$). The isolated black circle denotes the reference vortex ring value. Connecting lines are for visualization purposes only.

the turbulence energy per unit volume is deduced by multiplying the observed vortex length per volume times the energy per unit length; by integrating the velocity field of a straight vortex filament, the energy per unit length is estimated to be $E/L \approx \Gamma^2/(4\pi^2)\ln(b/a)$, where $b \approx \Lambda^{-1/2}$ is the typical distance between vortices. Our results show that for highly bent vortex filaments (as in the case of superfluid turbulence, where vorticity is even fractal [39]), E/L is certainly not constant.

D. Helicity

It is interesting to investigate the effects of topology by exploring the interplay of geometric and topological aspects on the dynamics and the kinetic helicity of the system. For this let us consider Fig. 7, where the velocity of a torus knot and that of the corresponding unknot (with same number of

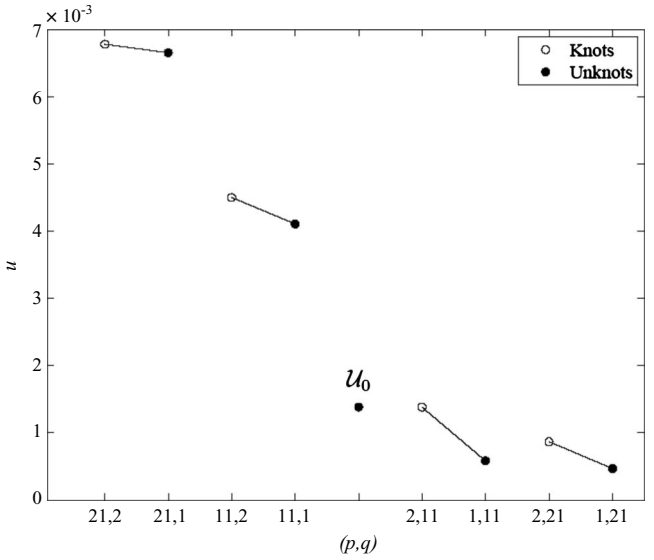

FIG. 7. Translational velocity u of knots and unknots shown for comparison. In general knots travel faster than their corresponding unknots. The isolated black circle denotes the reference vortex ring value. Connecting lines are for visualization purposes only.

longitudinal or meridian wraps) are shown for comparison. As we see in general vortex knots travel faster than their corresponding unknots; moreover, the higher is the number of longitudinal wraps p the faster is the translational motion, whereas the higher is q the slower is the propagation speed.

As far as helicity is concerned, from the values of Tables I and II and from Eq. (12) we immediately see that H increases with knot (and unknot) complexity, proportionately with $Lk=pq$. From the helicity decomposition in writhe and twist contributions [Eq. (12)], we see that for "poloidal" representations of knots, that is for $\mathcal{T}_{p,q}$ with $q>p$, writhe and twist helicity increase proportionately with the relative number of wraps, whereas for "toroidal" representations of knots, such as those given by the $\mathcal{T}_{p,2}$ ($p>2$), twist helicity remains almost constant, and any increase in linking number is mostly reflected in an increase in writhe helicity.

For vortex unknots, since the reference helicity of a vortex ring is set to $H=0$ ($Lk=0$), we have equal share of writhe and twist helicity.

E. Structural stability considerations

Aspects of structural stability of vortex knots and unknots based on permanence of knot signature and occurrence of a reconnection event are explored. In previous work we noticed the stabilizing effect of the BS law on LIA-unstable knots [17]. Here we extend this comparison to the knots and unknots considered. In general a vortex structure is deemed to be structurally stable if it evolves under conservation of topology, geometric signature and vortex coherency. Let us consider the results reported in the Tables I and II and shown in Fig. 8.

Since our results concern both Euler's and superfluid dynamics, it is important to remark that superfluid vortices can reconnect with each other in absence of dissipation [40,41],

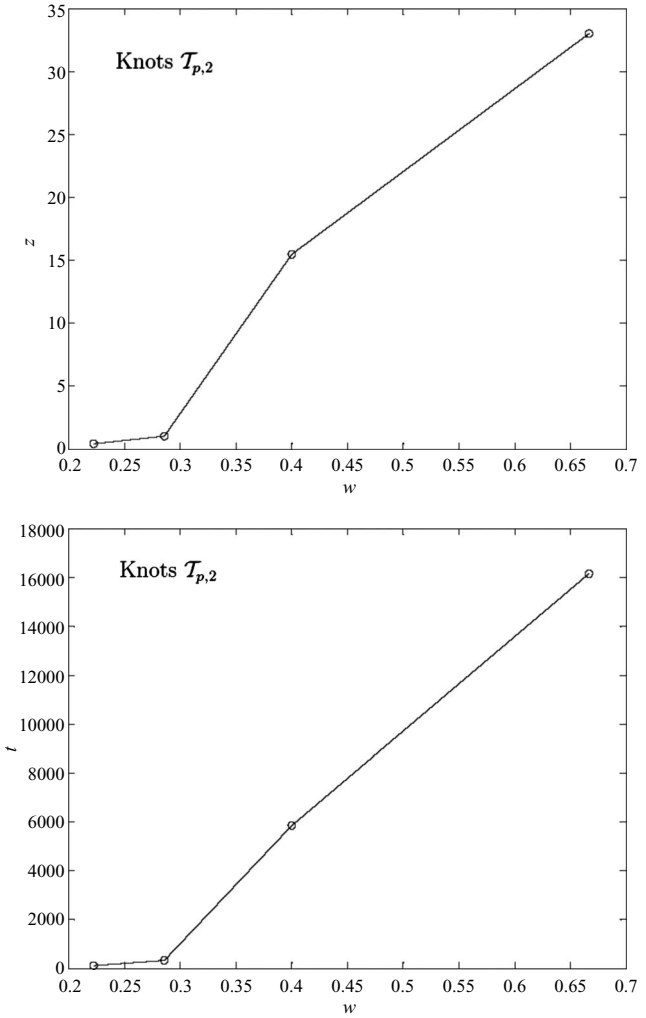

FIG. 8. Space traveled (z) and time elapsed (t) before a reconnection event takes place for torus knots $\mathcal{T}_{p,2}$ ($p=3,5,7,9$) plotted against the winding number w. Calculations are based on the Biot-Savart law. Connecting lines are for visualization purposes only.

whereas in the Euler context vortex topology is conserved; this important difference has been recently reviewed by Barenghi [42]. Here we adopt the following criterium: when, during the evolution, a vortex reconnection takes place, we stop the calculation, and deem the vortex to be structurally unstable. The last columns of the Tables I and II refer to the occurrence of a reconnection event at instant t. In the absence of a reconnection, we report the distance z traveled by the vortex during the computational time t. If z is much larger than the typical vortex size, then the knot/unknot tested is said to be structurally stable.

From the data of Table I we see that for $w<1$ the space traveled tends to decrease with increasing knot complexity: for example, $t(\mathcal{T}_{3,2}) \gg t(\mathcal{T}_{9,2})$. This behavior is also shown in Fig. 8. Note that knots with $w<1$ are LIA-unstable. Thus, the stabilizing effect due to the BS law is confirmed: all knots tested for which $w<1$ can indeed travel a distance which is larger than their size, before unfolding and reconnecting.

V. CONCLUSIONS

In this paper we examined the effect of several geometric and topological aspects on the dynamics and energetics of vortex torus knots and unknots (i.e., toroidal and poloidal coils). This study is carried out by numerically integrating the Biot-Savart law, and by comparing results for several knots and unknots for different winding numbers w. Generic behaviors are found for the class of knots/unknots tested, and main results are presented by normalizing velocity and energy by the corresponding value of a standard vortex ring ($\mathcal{U}_0$) of same size and circulation.

In general, for $w<1$ (where the number of longitudinal wraps is larger than that of meridian wraps) the more complex the vortex structure is, the faster it moves, and both torus knots and toroidal coils move faster than $\mathcal{U}_0$. For $w>1$ (where the relative number of meridian wraps dominates) all vortex structures move essentially as fast as $\mathcal{U}_0$, almost independently from their total twist. Therefore, in all cases total twist provides only a second-order effect on the dynamics.

We have also found that for $w<1$ vortex structures carry more kinetic energy than $\mathcal{U}_0$, whereas for $w>1$ knots and poloidal coils have almost the same energy as $\mathcal{U}_0$. The LIA law (an approximation often used to replace the Biot-Savart law, computationally more expensive) tend to underestimate the energy of knots with $w<1$ and to overestimate the energy of knots with $w>1$. Kinetic helicity, that admits decomposition in writhe and twist contributions, increases with knot complexity determined by the relative number of longitudinal and meridian wraps present, the latter contributing to the twist helicity rather modestly.

Finally, by extending previous results, we can confirm the stabilizing effect of the Biot-Savart law for knots with $w<1$, LIA-unstable: all knots tested have been found to be structurally stable regardless of the value of w, being able to travel in the fluid for several diameters before eventually unfolding and reconnecting.

[1] W. T. Thomson, Philos. Mag. **10**, 155 (1880).
[2] J. J. Thomson, *A Treatise on the Motion of Vortex Rings* (MacMillan and Co., London, 1883).
[3] Y. Fukumoto and H. K. Moffatt, Physica D **237**, 2210 (2008).
[4] Y. Hattori and Y. Fukumoto, Phys. Fluids **21**, 014104 (2009).
[5] F. Kaplanski, S. S. Sazhin, and Y. Fukumoto, J. Fluid Mech. **622**, 233 (2009).
[6] C. F. Barenghi, R. Hanninen, and M. Tsubota, Phys. Rev. E **74**, 046303 (2006).
[7] L. Kiknadze and Yu. Mamaladze, J. Low Temp. Phys. **126**, 321 (2002).
[8] R. L. Ricca, Physica D **237**, 2223 (2008).

[9] C. F. Barenghi and Y. A. Sergeev, Phys. Rev. B **80**, 024514 (2009).
[10] G. P. Bewley and K. R. Sreenivasan, J. Low Temp. Phys. **156**, 84 (2009).
[11] A. I. Golov and P. M. Walmsley, J. Low Temp. Phys. **156**, 51 (2009).
[12] P. M. Walmsley, A. I. Golov, H. E. Hall, A. A. Levchenko, and W. F. Vinen, Phys. Rev. Lett. **99**, 265302 (2007).
[13] T.-L. Horng, C.-H. Hsueh, and S.-C. Gou, Phys. Rev. A **77**, 063625 (2008).
[14] P. M. Mason and N. G. Berloff, Phys. Rev. A **79**, 043620 (2009).
[15] M. Tsubota and M. Kobayashi, J. Low Temp. Phys. **150**, 402 (2008).
[16] F. Maggioni, S. Z. Alamri, C. F. Barenghi, and R. L. Ricca, Il Nuovo Cimento C **32**, 133 (2009).
[17] R. L. Ricca, D. C. Samuels, and C. F. Barenghi, J. Fluid Mech. **391**, 29 (1999).
[18] R. G. K. M. Aarts and A. T. A. M. de Waele, Phys. Rev. B **50**, 10069 (1994).
[19] C. F. Barenghi, G. G. Bauer, D. C. Samuels, and R. J. Donnelly, Phys. Fluids **9**, 2631 (1997).
[20] K. W. Schwarz, Phys. Rev. B **38**, 2398 (1988).
[21] M. Tsubota, C. F. Barenghi, and T. Araki, J. Low Temp. Phys. **134**, 471 (2004).
[22] C. F. Barenghi, W. F. Vinen, and R. J. Donnelly, J. Low Temp. Phys. **52**, 189 (1983).
[23] P. G. Saffman, *Vortex Dynamics* (Cambridge University Press, Cambridge, England, 1992).
[24] R. L. Ricca and M. A. Berger, Phys. Today **49**(12), 28 (1996).
[25] L. S. Da Rios, Rend. Circ. Mat. Palermo **22**, 117 (1906).
[26] R. J. Arms and F. R. Hama, Phys. Fluids **8**, 553 (1965).
[27] R. L. Ricca, Fluid Dyn. Res. **18**, 245 (1996).
[28] G. K. Batchelor, *An Introduction to Fluid Dynamics* (Cambridge University Press, Cambridge, England, 1967).
[29] S. Kida, J. Fluid Mech. **112**, 397 (1981).
[30] R. L. Ricca, Chaos **3**, 83 (1993); **5**, 346(E) (1995).
[31] R. L. Ricca, in *Small-Scale Structures in Three-Dimensional Hydro and Magnetohydrodynamics Turbulence*, Lecture Notes in Physics Vol. 462, edited by M. Meneguzzi *et al.* (Springer-Verlag, Berlin, 1995), p. 99.
[32] F. B. Fuller, Proc. Natl. Acad. Sci. U.S.A. **68**, 815 (1971).
[33] R. L. Ricca and H. K. Moffatt, in *Topological Aspects of the Dynamics of Fluids and Plasmas*, edited by H. K. Moffatt *et al.* (Kluwer, Dordrecht, 1992), p. 225.
[34] S. Z. Alamri, Ph.D. thesis, Newcastle University, 2009.
[35] S. Z. Alamri, A. J. Youd, and C. F. Barenghi, Phys. Rev. Lett. **101**, 215302 (2008).
[36] R. L. Ricca, in *Lectures on Topological Fluid Mechanics*, Springer-CIME Lecture Notes in Mathematics Vol. 1973, edited by R. L. Ricca (Springer-Verlag, Berlin, 2009), p. 169.
[37] C. F. Barenghi, R. L. Ricca, and D. C. Samuels, Physica D **157**, 197 (2001).
[38] D. Kivotides, J. C. Vassilicos, D. C. Samuels, and C. F. Barenghi, Phys. Rev. Lett. **86**, 3080 (2001).
[39] D. Kivotides, C. F. Barenghi, and D. C. Samuels, Phys. Rev. Lett. **87**, 155301 (2001).
[40] G. P. Bewley, M. S. Paoletti, K. R. Sreenivasan, and D. P. Lathrop, Proc. Natl. Acad. Sci. U.S.A. **105**, 13707 (2008).
[41] J. Koplik and H. Levine, Phys. Rev. Lett. **71**, 1375 (1993).
[42] C. F. Barenghi, Physica D **237**, 2195 (2008).